Creation of Nanohillocks on CaF₂ Surfaces by Single Slow Highly Charged Ions

A. S. El-Said,[1,*] R. Heller,[2] W. Meissl,[1] R. Ritter,[1] S. Facsko,[2] C. Lemell,[3] B. Solleder,[3] I. C. Gebeshuber,[1] G. Betz,[1] M. Toulemonde,[4] W. Möller,[2] J. Burgdörfer,[3] and F. Aumayr[1,†]

[1]*Institut für Allgemeine Physik, Vienna University of Technology, 1040 Vienna, Austria, EU*
[2]*Forschungszentrum Dresden-Rossendorf, D-01328 Dresden, Germany, EU*
[3]*Institute for Theoretical Physics, Vienna University of Technology, 1040 Vienna, Austria, EU*
[4]*CIMAP, ENSICAEN, CEA, CNRS, University of Caen, 14070 Caen, France, EU*

Upon impact on a solid surface, the potential energy stored in slow highly charged ions is primarily deposited into the electronic system of the target. By decelerating the projectile ions to kinetic energies as low as $150 \times q$ eV, we find first unambiguous experimental evidence that potential energy alone is sufficient to cause permanent nanosized hillocks on the (111) surface of a CaF₂ single crystal. Our investigations reveal a surprisingly sharp and well-defined threshold of potential energy for hillock formation which can be linked to a solid-liquid phase transition.

PACS numbers: 79.20.Rf, 34.35.+a, 61.80.Jh

High-energy photons, electrons, and ions are frequently employed as tools to lithographically modify surfaces on the nanometer scale. Among them, ion beams are, perhaps, still the least developed technique in the field of nanolithography, in part due to the fact that many fundamental aspects of their interactions with the surface are not yet well understood. Three techniques, focused ion beam, proton beam writing, and ion projection lithography, have now breached the technologically difficult 100 nm barrier and are capable of fabricating structures on the nanoscale [1]. Current research in the field of advanced ion-beam techniques focuses on the energy and charge state dependence of the primary beam. While the interaction of intense beams of keV ions with surfaces can result in well-ordered patterns, such as ripples or self-ordered dots [2–4], drastic modifications to the surface topography by individual ions are induced only if the material is exposed to energetic ions (MeV to GeV region). At these high impact energies, the energy deposition leads to the creation of nanosized hillocks or craters randomly distributed on the surface. Recently, the formation of multiple, regularly spaced nanodots on SrTiO₃ surfaces has been demonstrated for single swift Xe ion impact under grazing angles of incidence [5].

One major limitation for the application of swift heavy ions to three-dimensional structure formation is the radiation damage of deeper layers. The desire to confine the energy deposition to the surface layer has stimulated the interest in slow (eV to keV) and highly charged ions. With increasing charge state, these ions carry an increasingly large amount of potential energy (e.g., 14 keV for bare Ar^{18+} and 51 keV for Ne-like Xe^{44+}). The potential-energy deposition and electron depletion induced by the neutralization sequence of slow highly charged ions (HCI) on insulator targets is expected to be confined to a nanometer-sized volume close to the surface and to occur on a femtosecond time scale [6]. Intuitively, one expects

the formation of nanosized surface craters due to Coulomb explosion. In contrast to these expectations, the first experiments with $7q$ keV HCI (q denoting their incident charge state) on Muscovite mica showed nanohillocks [7,8] when the interaction zone was inspected by atomic force microscopy (AFM). For ion charge states below $q = 30$, no damage could be identified. Systematic experiments on mica revealed that the observed structures do not represent topographic changes of the surface but rather changes in the surface friction leading to the observation of "hillocks" and sometimes "craters" depending on the scanning direction of the AFM [8]. Furthermore, the observed structures disappeared after repeated scanning with AFM. The volume of the "apparent" structures was found to be roughly proportional to the potential energy of the impinging ions [8,9] while only weakly dependent on the projectile kinetic energy [9]. Studies on other surfaces (such as highly oriented pyrolytic graphite) found similar results (for a recent review of this field, see [10]). However, due to the high kinetic energy of the projectile ions (up to several hundred keV as a result of 5–10 kV acceleration voltage), kinetic effects (e.g., contributions from kinetic energy transfer to the target cores or electrons) could not be ruled out.

In this Letter, we present experiments with *very slow* (down to $v_p \approx 0.03$ a.u. or 30 eV/amu) HCI creating hillocklike topographic nanostructures on the surface of CaF₂ single crystals which are stable in air and nonerasable by AFM scanning. Surprisingly, these nanostructures closely resemble those created by swift heavy ions at the surface [11] while leaving deeper layers of the target undamaged. Moreover, we find a strong dependence of the formation on the potential energy rather than on the kinetic energy with a sharp and well-defined threshold of potential energy required for the onset of nanohillock formation. Simulations of the dissipation of potential energy into the target material on the basis of an extended

classical over-the-barrier model have been performed to facilitate the interpretation of the experimental findings. Since CaF$_2$ is used as an insulator in silicon microelectronic devices [12,13] epitaxially grown on semiconductor surfaces [14], our findings might be of importance for high resolution patterning of thin CaF$_2$ films on Si and for the creation of nanostructured templates for adlayer growth during fabrication of CaF$_2$/Si-based epitaxial insulator-semiconductor structures.

Our experiments were performed on air-cleaved CaF$_2$(111) single crystal surfaces. Cleavage is known to result in a fluorine-terminated surface which is stable in air. Contact-mode AFM in UHV revealed large atomically flat surfaces with occasional cleavage steps separating individual terraces. Irradiation of CaF$_2$ samples (freshly cleaved before their transfer into a vacuum chamber of pressure in the 10^{-10} mbar range) took place at the ion-beam center of Forschungszentrum Dresden-Rossendorf. Isotope-pure ^{129}Xe^{q+} ions ($q = 24$–36) were extracted from a Dresden electron beam ion trap source [15] and decelerated by a two-stage deceleration system to the desired final impact energy before impinging onto the single crystal CaF$_2$ surface under a normal angle of incidence. Deceleration to a final potential difference between source and target down to 150 V resulted in the lowest impact energies of $150q$ eV (150 V times projectile charge q), i.e., an impact energy of only 28–42 eV per atomic mass unit. The time-averaged beam flux varied between 10^4 and 10^6 ions/s. After exposure to fluences of about 10^{10} ions/cm^2, the crystal was transferred to an UHV-AFM/STM (Omicron) and inspected by contact-mode AFM.

A typical AFM topographic image of a CaF$_2$(111) surface (Fig. 1) after irradiation with $2q$ keV Xe^{33+} ions (~ 500 eV/amu) displays hillocklike nanostructures protruding from the surface. The AFM images were evaluated in terms of their areal density, height, and width distributions of the hillocks. The hillocks in Fig. 1 are typically 20 nm in diameter and 0.8 nm in height. Because of the finite radius of curvature of the AFM tip (nominally 7–10 nm), the diameter of the hillocks is subject to a systematic error [11]. Measurements of heights of structures, however, are known to be reasonably accurate. From the
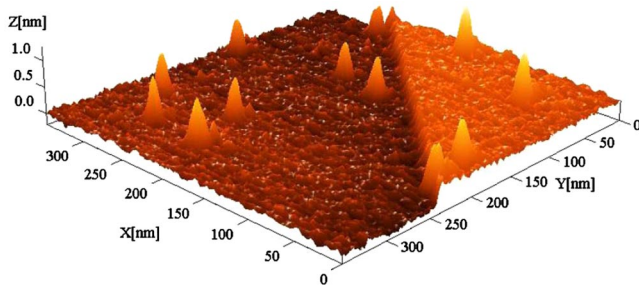
number of hillocks per unit area and the applied ion fluence, we determine that a vast majority of projectiles (about 80% ± 10%) produce one hillock each.

To demonstrate that the hillocks are solely due to the deposition of potential rather than kinetic energy (in the form of nuclear or electronic stopping) of the projectiles, we decelerated the Xe^{33+} ions to final impact energies as low as 38 eV/amu ($150q$ eV). In Fig. 2, we show the measured mean volume of the hillocklike nanostructures on CaF$_2$ produced by the impact of Xe^{33+} projectile ions as a function of their kinetic energy together with previous results for much more energetic ($10q$ keV) Xe^{33+} ions [16]. Despite the reduction of the kinetic energy by almost 2 orders of magnitude, the measured hillock volume is essentially unaffected and stays almost constant. The data might even indicate a slight increase with decreasing kinetic energy, a trend that was also found for other charge states (cf. Fig. 3).

In order to explore the dependence on the potential energy of the projectiles, we employ Xe^{q+} ions with charge states ranging from $q = 24$ to $q = 36$ while leaving the potential difference between the ion source and target surface at a constant value of 150 V. The hillock volume was found to be strongly dependent on the potential energy of the projectiles (Fig. 3). A remarkably well-defined sharp threshold in potential energy (between 10.4 keV for Xe^{27+} and 12.0 keV for Xe^{28+}) for hillock formation emerges. Above this threshold, an increase of the potential energy leads to a strong increase of hillock volume. The hillock volume seems to increase slightly for decreasing kinetic energy, and the threshold shifts by about 2 keV. Repeated measurements confirmed that hillocks are produced by slow ($150q$ eV) Xe^{28+} but not for fast ($10q$ keV) Xe^{28+} projectiles. While above the threshold the hillock volume increases linearly with potential energy, the shape of the
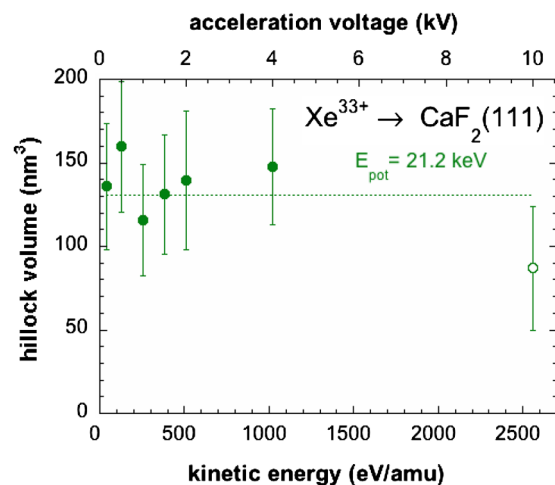

FIG. 1 (color online). Topographic contact-mode AFM image of a CaF$_2$(111) surface after irradiation with $2q$ keV Xe^{33+} ions showing hillocklike nanostructures protruding from the surface.

FIG. 2 (color online). Mean volume of hillocklike nanostructures on CaF$_2$ produced by the impact of Xe^{33+} projectile ions as a function of their kinetic energy. Solid symbols: Present results; open symbol: result from Ref. [16].
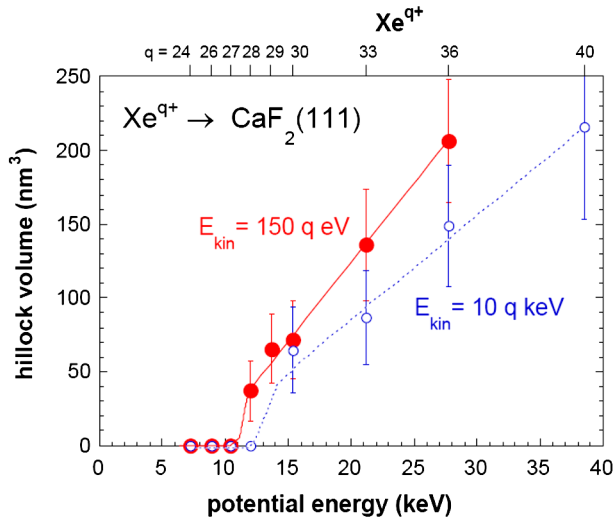
FIG. 3 (color online). Mean volume of hillocklike nanostructures as a function of the potential energy of Xe^{q+} projectiles. Solid symbols correspond to measurements taken at $150q$ eV impact energies, while open symbols show the results taken for $10q$ keV. Hillocks are found only above a potential-energy threshold which slightly shifts with kinetic energy. Lines are drawn to guide the eye. The error bars represent the statistical variation of the actual hillock volume and are not due to limited resolution of our AFM.

hillocks does not depend on beam parameters; also the base diameter shows only a small dependence on the potential energy of the projectile.

Surprisingly, the hillocks observed in our experiment resemble the surface structures generated by swift heavy ions. For the latter, hillock formation was observed above an energy loss of 5 keV/nm [11] which results from 500 eV/nm nuclear stopping S_n and 4.5 keV/nm electronic stopping S_e [17]. While S_n corresponds to direct transfer of kinetic energy into lattice heating, i.e., excitation of phonons along the projectile trajectory, S_e is a measure for the excitation of the electronic subsystem of the target. It acts as a precursor for lattice excitation via electron-phonon coupling [18]. By contrast, for very slow highly charged ions (kinetic energy of about 5 keV for $150q$ eV Xe^{33+}), the total stopping power amounts to only 1.3 keV/nm with a less than 5% contribution from S_e. Deposition of the potential energy (E_{pot}) of the highly charged projectile, 75% of which is stored in the target material [19], must therefore play a decisive role for slow HCI. However, as the potential-energy threshold was found around 12 keV (see Fig. 3), it is obvious that only part of E_{pot} is effectively converted into lattice excitations.

In the following, we present simulations of the energy transfer from the HCI to the lattice of the CaF_2 target combining above and below surface electron emission processes along the projectile trajectory [20] with electron transport within the target material including the generation of secondary electrons and heating of the crystal

lattice [21]. This sequence involves a twofold conversion of energy: First, potential energy is converted into kinetic energy of emitted primary electrons. In turn, electrons deposit their energy in the crystal as heat, eventually leading to melting of the material.

Highly charged ions approaching solid surfaces undergo a large number of neutralization and deexcitation processes which are well described within the classical-over-barrier model developed for metal surfaces [22] and its extension for insulator targets [20]. Electrons from the target are transferred into highly excited states of the projectile which may decay by collisional, radiative, and Auger processes. Transfer of electrons to the projectile leaves unbalanced holes (F^0 atoms) in the surface which store part of the potential energy carried into the collision. Upon impact of the projectile, the target is structurally weakened.

Projectiles reach the surface far from ground state as the time spent in front of the surface is not sufficient for a complete relaxation. At this stage, electrons are captured into moderately excited states by either resonant charge transfer from the valence band or Auger neutralization processes followed by an Auger deexcitation sequence. Along this sequence, electrons with low to intermediate energies up to a few hundred eV are emitted. If inner-shell holes are to be filled (e.g., in the cases of Ar^{17+} and Ar^{18+} [16]), electrons with keV kinetic energies are released. The potential energy stored in the incoming HCI will be deposited along the first few nanometers of its trajectory below the target surface. The kinetic energy of the projectile determines the depth within which the neutralization is completed (~1 nm for $150q$ eV and ~4 nm for $10q$ keV projectiles; see Fig. 4). It is much smaller than the total range of the ion in the solid (~6 nm for $150q$ eV and ~90 nm for $10q$ keV projectiles [17]).

For an HCI with $q = 40$, we estimate about 250 unbalanced holes [23] created in the course of the interaction of a single ion affecting the crystal structure of the target. In our electron-transport simulation, elastic and inelastic scatter-
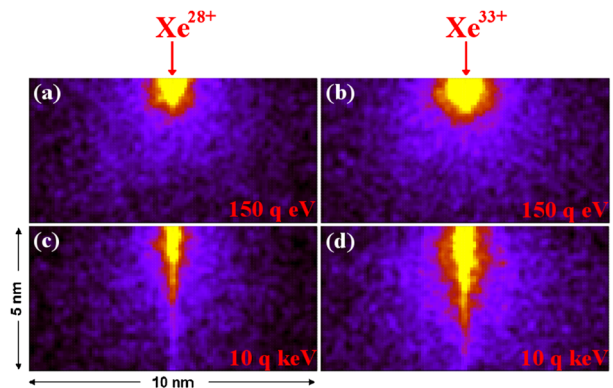

FIG. 4 (color online). Energy density deposited by Xe^{28+} (a),(c) and Xe^{33+} (b),(d) projectile ions in a CaF_2 crystal. Calculations were performed for impact energies of $150q$ eV (a),(b) and $10q$ keV (c),(d). For details, cf. the text.

ing processes are taken into account, leading to the creation of secondary electrons (whose trajectories are followed as well) and to excitations of phonons in the interaction with the crystal atoms. Energy transfer to the lattice will eventually lead to heating and melting of the crystal. As a consequence of the high-energy density required for melting of a CaF_2 crystal (~ 0.55 eV/atom), low-energy electrons contribute more efficiently to the melting process than high-energy electrons, which distribute their energy over a much larger volume because of their larger inelastic and elastic mean free paths [21]. Contrary to naive expectations and quite surprisingly, the decisive difference between below and above threshold charge states is not the additional fast Auger electron but the many additional slow electrons emitted along the deexcitation sequence resulting from the filling of the additional inner-shell hole.

The average energy density deposited in the target along the trajectory as a function of the distance from the projectile track features a "hot" core (bright yellow region in Fig. 4) in which the critical energy density required for melting is reached. The shape of this volume strongly depends on the velocity of the projectile. While for slow projectiles the volume is almost hemispherical, fast projectiles create an elongated volume resembling the shape of a candle flame. If either the velocity is increased or the potential energy is reduced (smaller initial charge states), the diameter of the heated volume shrinks. While the present electron-transport simulation assuming a structureless medium cannot account for effects of the crystalline structure, important information on the spatial distribution of energy deposition into the electronic degrees of freedom preceding structure modification and melting can be inferred: A minimum volume heated above the threshold energy density of 0.55 eV/atom is needed for restructuring and hillock formation. The core volume in Fig. 4(a) is found to be about 2.5 nm^3 or, equivalently, about 15 unit cells of CaF_2 (lattice constant of $a = 5.462$ Å) containing about 10^2 atoms. Equally important is the (smallest) linear dimension of the hot core. Only if the diameter of the core exceeds the size of the unit cell can the above-critical energy density be retained for a sufficiently long time such that the relatively slow processes of restructuring and melting occur before cooling sets in. Hillock formation was experimentally observed for all cases displayed in Fig. 4 except for Fig. 4(c) (Xe^{28+}, $10q$ keV) in which the diameter of the core region is reduced to about the lattice constant. In this case, the deposited energy is apparently dissipated too quickly, and the melting process is suppressed. Clearly, future simulations must be extended from the present multifemtosecond to the multipicosecond scale by employing molecular-dynamics techniques to quantify the melting process in more detail.

In conclusion, we have shown for the first time that the potential energy of highly charged ions can be exclusively responsible for the production of permanent nanosized hillocks on insulating CaF_2 single crystals. Accompanying simulations of the energy density deposited on the target atoms suggest a link of observable surface modifications to a solid-liquid phase transition. They are also able to qualitatively explain the existence and shift of the threshold charge state for hillock formation observed for projectiles with different kinetic energies.

*Permanent address: Physics Department, Mansoura University, 35516 Mansoura, Egypt.
†To whom correspondence should be addressed.
aumayr@iap.tuwien.ac.at

[1] F. Watt *et al.*, Int. J. Nanosci. **4**, 269 (2005).
[2] S. Facsko *et al.*, Science **285**, 1551 (1999).
[3] M. Castro *et al.*, Phys. Rev. Lett. **94**, 016102 (2005).
[4] B. Ziberi *et al.*, Phys. Rev. B **72**, 235310 (2005).
[5] E. Akcoltekin *et al.*, Nature Nanotechnology **2**, 290 (2007).
[6] A. Arnau *et al.*, Surf. Sci. Rep. **27**, 113 (1997).
[7] D. H. Schneider *et al.*, Radiat. Eff. Defects Solids **127**, 113 (1993); D. Schneider *et al.*, Surf. Sci. **294**, 403 (1993).
[8] C. Ruehlicke, M. A. Briere, and D. H. Schneider, Nucl. Instrum. Methods Phys. Res., Sect. B **99**, 528 (1995).
[9] D. C. Parks *et al.*, J. Vac. Sci. Technol. B **13**, 941 (1995).
[10] F. Aumayr, A. S. El-Said, and W. Meissl, Nucl. Instrum. Methods Phys. Res., Sect. B (in press).
[11] N. Khalfaoui *et al.*, Nucl. Instrum. Methods Phys. Res., Sect. B **240**, 819 (2005).
[12] T. P. Smith *et al.*, Appl. Phys. Lett. **45**, 907 (1984).
[13] L. J. Schowalter and R. W. Fathauer, J. Vac. Sci. Technol. **4**, 1026 (1986).
[14] C. A. Lucas and D. Loretto, Appl. Phys. Lett. **60**, 2071 (1992).
[15] F. Grossmann *et al.*, Nucl. Instrum. Methods Phys. Res., Sect. B **256**, 565 (2007).
[16] A. S. El-Said *et al.*, Nucl. Instrum. Methods Phys. Res., Sect. B **258**, 167 (2007).
[17] J. F. Ziegler, J. P. Biersack, and U. Littmark, *The Stopping and Range of Ions in Solids* (Pergamon Press, New York, 1985); http://www.srim.org.
[18] M. Toulemonde, C. Dufour, and E. Paumier, Phys. Rev. B **46**, 14 362 (1992); A. Meftah *et al.*, Nucl. Instrum. Methods Phys. Res., Sect. B **237**, 563 (2005).
[19] D. Kost *et al.*, Phys. Rev. Lett. **98**, 225503 (2007).
[20] L. Wirtz *et al.*, Phys. Rev. A **67**, 012903 (2003).
[21] C. Lemell *et al.*, Solid-State Electron. **51**, 1398 (2007).
[22] J. Burgdörfer, P. Lerner, and F. W. Meyer, Phys. Rev. A **44**, 5674 (1991).
[23] W. Meissl *et al.*, e-J. Surf. Sci. Nanotech. **6**, 54 (2008).